Facies (2021) 67:19
https://doi.org/10.1007/s10347-021-00630-3

ORIGINAL ARTICLE

Ribbon rocks revisited: the upper Cambrian (Furongian) Hwajeol Formation, Taebaek Group, Korea

Jeong-Hyun Lee[1] · Se Hyun Cho[2] · Da Young Jung[2] · Suk-Joo Choh[2] · Dong-Jin Lee[3]

Received: 22 October 2020 / Accepted: 4 May 2021 / Published online: 15 May 2021
© Springer-Verlag GmbH Germany, part of Springer Nature 2021

Abstract

Alternations of thin-bedded limestone and shale, or ribbon rock, commonly occur throughout lower Palaeozoic carbonate successions; however, their formative processes are still unclear. In this study, we discuss the origin of the ribbon rocks of the upper Cambrian Hwajeol Formation, Korea, based on detailed microfacies analysis of a ~ 2-m-thick interval. Five sedimentary microfacies were identified: normally graded calcarenite to shale; parallel-laminated shale; lime mudstone; wackestone-to-packstone; and bioclastic–intraclastic packstone-to-conglomerate. Shale facies were most likely formed by frequent storm-induced bottom currents, whereas, lime mudstone facies were deposited in situ by suspension settling of micrite, mudflows, or growth of keratose sponges on the seafloor, and/or formed by early diagenetic growth. Conglomerate/packstone/wackestone indicate infrequent, larger-scale events, e.g., mega-storms, tsunamis, or earthquakes. We propose a new formative model for tempestite-type ribbon rock based on the Hwajeol example, and suggest that this model can be differentiated from the other types of ribbon rocks—tidalite, turbidite, and diagenetic types. Formation of the tempestite-type ribbon rocks would have been promoted by the characteristic environmental conditions of the early Palaeozoic, in particular sea-water chemistry that promoted calcite precipitation and the paucity of burrowers. Detailed microscopic observations can thus provide clues to elucidate previously unknown sedimentary processes in the deeper parts of carbonate platforms.

Keywords Early Palaeozoic · Ribbon rock · Ribbon carbonate · Parted limestone · Limestone–shale interlayer

Introduction

Ribbon rock is characterised by alternations of thin-bedded (or nodular) lime mudstone and shale/marlstone (Reinhardt and Hardie 1976; Cook and Taylor 1977; Markello and Read 1981; Demicco 1983). The name originated from the ribbon-like appearance of the thin alternating beds, which is enhanced in the field by differential weathering. The term "ribbon rock" was adopted by sedimentologists in the 1940s, particularly by local geologists working in the central Appalachian region (White 1943). This characteristic lithofacies occurs throughout certain geological intervals, such as the lower to middle Palaeozoic and Mesozoic (Flügel 2004; Westphal et al. 2008), but most commonly in lower Palaeozoic successions worldwide (e.g., Markello and Read 1981; Demicco 1983; Pratt and James 1986; Chow and James 1987; Coniglio and James 1990; Sepkoski et al. 1991; Elrick and Snider 2002; Kwon et al. 2006; Chen et al. 2010, 2011; Bayet-Goll et al. 2015).

Several different types of sedimentary facies have been described as ribbon rock or similar names, such as parted

✉ Suk-Joo Choh
sjchoh@korea.ac.kr

Jeong-Hyun Lee
jeonghyunlee@cnu.ac.kr

Se Hyun Cho
whtpgus307@korea.ac.kr

Da Young Jung
momokite@korea.ac.kr

Dong-Jin Lee
lichenaria@daum.net

[1] Department of Geological Sciences, Chungnam National University, Daejeon 34134, Republic of Korea

[2] Department of Earth and Environmental Sciences, Korea University, Seoul 02841, Republic of Korea

[3] College of Earth Sciences, Jilin University, Changchun 130061, China

limestone (Chow and James 1987; Coniglio and James 1990), ribbon carbonate (Markello and Read 1981; Moshier 1986; Cowan and James 1992; Adams and Grotzinger 1996), limestone–shale/marl couplets/alternations/interlayers (Munnecke and Samtleben 1996; Kwon et al. 2006; Westphal 2006; Chen et al. 2010), and rhythmite (Elrick and Snider 2002). Herein, we apply the most commonly used name for these rocks: ribbon rock. Many lower Palaeozoic ribbon rocks consist of nodular or thin-bedded (~ 1 cm) limestone alternating with shale (e.g., Markello and Read 1981). In contrast, middle–upper Palaeozoic and Mesozoic ribbon rocks are characterised by thicker-bedded (2–10 cm) alternating limestone and shale units (e.g., Westphal et al. 2008). The formative mechanisms and depositional environments of ribbon rocks varied from place to place and from time to time. They were deposited within environments ranging from supratidal to deep subtidal (e.g., Bayet-Goll et al. 2015), and could have been formed during early diagenesis by segregation of calcium carbonate from surrounding shale (Munnecke and Samtleben 1996; Westphal 2006; Westphal et al. 2008; Amberg et al. 2016; Nohl et al. 2019; Nohl and Munnecke 2019).

Ribbon rock is one of the most common sedimentary facies in lower Palaeozoic carbonate successions, and understanding the formation of ribbon rocks is essential to interpret early Palaeozoic environmental conditions. However, how the lower Palaeozoic ribbon rocks were formed has long been a matter of debate. Previous studies rather simply interpreted the lower Palaeozoic ribbon rocks as turbidites (Coniglio and James 1990), deep subtidal storm deposits (Pfeil and Read 1980; Markello and Read 1981; Elrick and Snider 2002; Chen et al. 2010; Bayet-Goll et al. 2015), or shallow subtidal to intertidal deposits (Demicco 1983; Bayet-Goll et al. 2015). Sepkoski et al. (1991) suggested that the thin limestone beds were formed as tempestites; whereas, the shales represented "muddy tails" following storms or hemipelagic sediments between storm events. However, recent studies of shales have revealed that currents are one of the most important mechanisms of transport and deposition of fine-grained siliciclastic sediments (Schieber and Yawar 2009; Trabucho-Alexandre et al. 2012; Egenhoff and Fishman 2013), suggesting that there are still many unsolved questions regarding the formative mechanisms of lower Palaeozoic ribbon rocks. In this study, we focus on a typical lower-Palaeozoic-type ribbon rock in the upper Cambrian (Furongian) Hwajeol Formation, Taebaek Group, Korea, to describe a new formative mechanism for ribbon rock. A better understanding of the sedimentological processes involved in ribbon rock formation yields new insights into early Palaeozoic sedimentary systems.

Geological setting and methods

During the early Palaeozoic, thick mixed carbonate–siliciclastic successions were deposited on the tectonically stable Sino-Korean Block that was located at the margin of Gondwana (Meng et al. 1997; McKenzie et al. 2011). In the eastern margin of the block, the Joseon Supergroup was deposited in the Taebaeksan Basin, Korea (Fig. 1). The supergroup is unconformably bound by Precambrian basement rocks below and the Carboniferous–Triassic Pyeongan Supergroup above (Chough 2013). The Taebaek Group, a subunit of the Joseon Supergroup, was deposited from Cambrian Series 2 to the Middle Ordovician and consists of ten lithostratigraphic units including the Hwajeol Formation (Fig. 2a) (Choi et al. 2004; Kwon et al. 2006).

The Hwajeol Formation, which has a maximum thickness of 200 m, was deposited throughout the Furongian (Kobayashi 1966; Cheong 1969). Ribbon rock with several intercalated flat-pebble conglomerate beds dominates the upper Hwajeol Formation (maximum thickness 120 m), and was deposited in an inner- to outer-ramp environment (Kwon et al. 2006; Byun and Kwon 2020). The upper Hwajeol Formation was formed during the late Jiangshanian–informal Stage 10 (ca. 4–5 Myr), indicated by the *Asioptychaspis*, *Quadraticephalus*, and *Eosaukia* trilobite biozones (Sohn and Choi 2005, 2007) and the *Proconodontus tenuiserratus*, *P. posterocostatus*, *P. muelleri*, *Eoconodontus notchpeakensis*, *Cambrooistodus minutus*, *Cordylodus proavus*, and *Fryellodontus inornatus–Monocostodus sevierensis–Semiacontiodus lavadamensis* conodont biozones (Jeong and Lee 2000; Lee and Seo 2008; Lee 2014).

This study was conducted at the Seokgaejae section, which is a type section of the Taebaek Group (Choi et al. 2004)

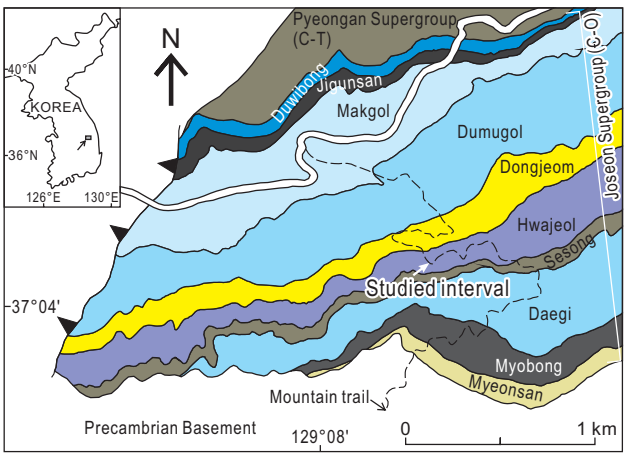

Fig. 1 Geological map of the study area (Seokgaejae section; 37°04′27″ N, 129°08′35″ E). Illustration modified after Choi et al. (2004)

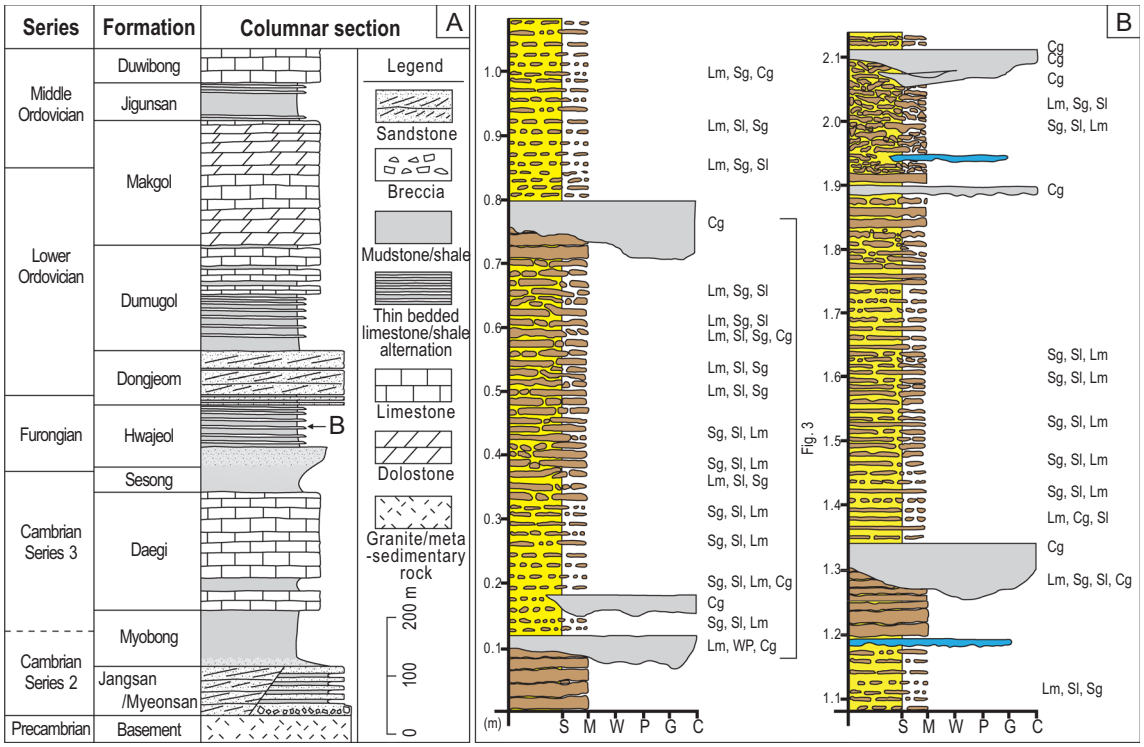

Fig. 2 **a** Summary of the litho- and chronostratigraphy of the Taebaek Group. Illustration modified after Lee et al. (2016a). **b** Detailed sedimentological log of the studied interval of the upper Hwajeol Formation. *Cg* bioclastic–intraclastic packstone-to-conglomerate, *Lm* lime mudstone, *Sg* normally graded calcarenite to shale, *Sl* parallel-laminated shale, *WP* wackestone-to-packstone. Yellow: shale, brown: lime mudstone, blue: skeletal grainstone, grey: limestone conglomerate. *S* shale, *M* lime mudstone, *W* wackestone, *P* packstone, *G* grainstone, *C* conglomerate

(Fig. 1). Detailed sedimentological logging was conducted of a ~ 2-m-thick interval located about 50 m below the upper boundary of the Hwajeol Formation (within the Unnamed Zone below *P. muelleri* Zone; Lee and Seo 2008) (Fig. 2). A total of 29 samples were collected, and 46 thin sections were prepared from these samples. In addition, continuous samples were collected from a 75.7-cm-thick succession within the 2-m-thick interval to obtain more detailed information (Fig. 2); these samples were prepared as four sets of serial thin sections (17 thin sections for each set; a total of 68 thin sections) for the purpose of detailed microfacies analysis (Fig. 3). In these thin sections, microscale sedimentary features such as component, ratio between limestone and shale, shape and geometry of limestone nodules, and sedimentary structures such as erosive surface, graded bedding, and parallel lamination are described. The areal percentage of each microfacies was calculated from the thin sections of the 75-cm-thick interval using ImageJ.

Ribbon rocks in the Hwajeol Formation

In the field, ribbon rocks are characterised by nodular (Fig. 4a, b) to bedded limestones (Fig. 4c, e) interbedded with shale that gradationally change from one to another. In some cases, sharp boundaries can be recognised within the shale (Fig. 4d). Conglomerate beds are occasionally intercalated with the ribbon rocks; these conglomerates exhibit lateral variations in thickness (Figs. 2b and 4f). From detailed microscale analysis, five microfacies were identified from the studied interval of the Hwajeol Formation on the basis of grain composition and sedimentary structures (Table 1). These microfacies are normally graded calcarenite to shale (facies Sg), parallel-laminated shale (facies Sl), lime mudstone (facies Lm), wackestone-to-packstone (facies WP), and bioclastic–intraclastic packstone-to-conglomerate (facies Cg). The occurrence

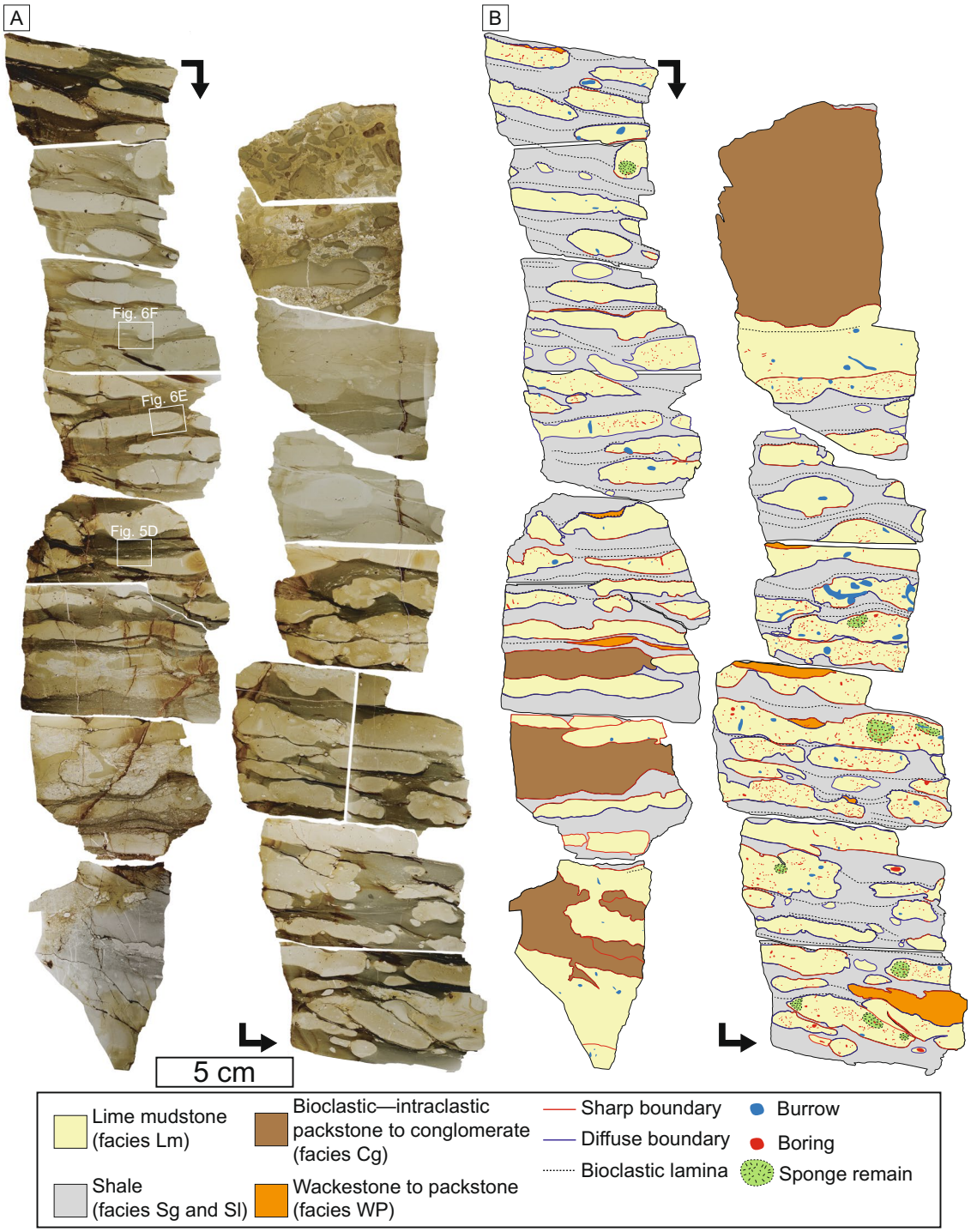

Fig. 3 **a** Photomicrographs of continuous thin sections through the 75-cm-thick interval and **b** their interpretative sketch. Note that bioturbation is concentrated within lime mudstone. Locations of some photomicrographs are marked on the thin sections

of each microfacies is generally less than 10 cm thick, and is commonly a few mm to 3 cm thick (Fig. 3). A total

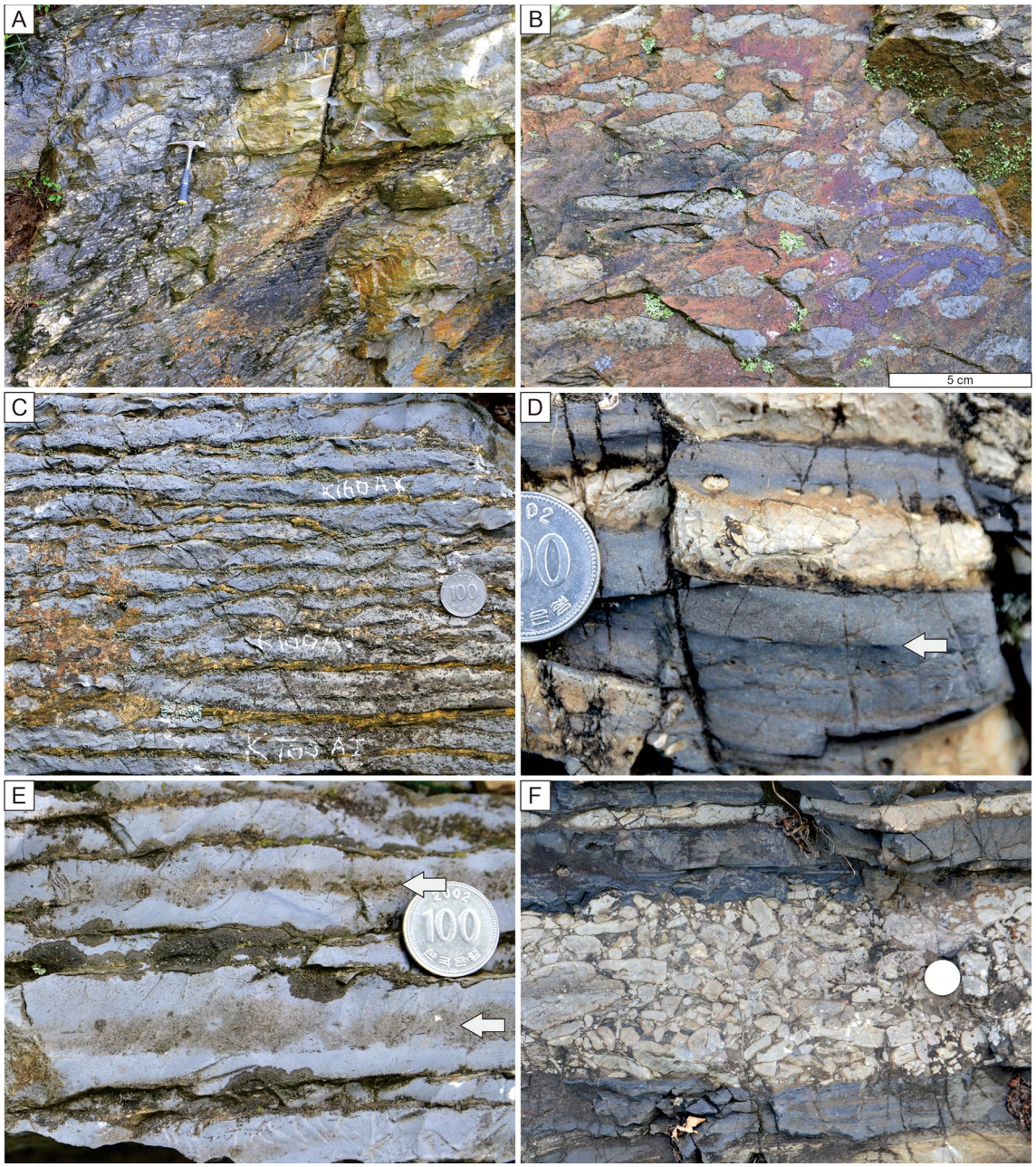

Fig. 4 Outcrop photographs of the Hwajeol Formation. **a** General lithology of the Hwajeol Formation, which is composed mainly of ribbon rock. Hammer for scale is 28 cm long. **b** Nodular ribbon rock. **c** Thin-bedded ribbon rock. **d** Close-up of the ribbon rock. Note the occurrence of a sharp boundary within shale (arrow). **e** Grainstone layers (arrowed) imbedded within the ribbon rock. **f** Flat-pebble conglomerate. The coin for scale in **c**–**f** is 23 mm in diameter

of 52 limestone–shale couplets (siliciclastic mudstone and overlying limestone nodules/layers) consisting of 96 nodular to thin-layered lime mudstones were described from the 75-cm-thick continuous-thin-section interval (Fig. 3).

Microfacies analysis

Normally graded calcarenite to shale (facies Sg)

Description The normally graded calcarenite to shale facies is characterised by a gradual transition from underlying silt- to sand-sized carbonate grains to overlying mud-sized grains with sporadic fragmented bioclasts (Fig. 5). Carbon-

Table 1 Summary of the sedimentary facies

Facies	Description	Interpretation
Normally graded calcarenite to shale (facies Sg)	Gradually fining upward from sand-sized bioclast to mud-sized particles; erosive lower boundary; differential compaction features	Weak storm-generated bottom current or distal turbidity current
Parallel laminated shale (facies Sl)	Mainly parallel-laminated mudstone; sometimes very thin bioclastic laminae at the base; gradually changes upward from underlying facies Sg	Non-turbulent lower energy flow evolved from storm current followed by hemipelagic sedimentation
Lime mudstone (facies Lm)	Thin bedded to nodular homogeneous micritic limestone; sharp to diffuse lower boundary; sharp upper boundary	Hemipelagic suspension settling of micrite/early diagenesis/in situ calcification of keratose sponge/rarely mudflow
Wackestone-to-packstone (facies WP)	Micritic clast and skeletal grains supported by the micritic matrix; sharp lower boundary; some channel-like geometry	Mud flow
Bioclastic–intraclastic packstone-to-conglomerate (facies Cg)	Flat micritic intraclasts and bioclastic grainstone matrix; showing horizontal- to cross-lamination; generally clast-supported; partly matrix-supported; sharp, channel-like lower boundary	Strong storm-generated bottom current or debris flow

ate grains mostly consist of fragmented or rounded fossil fragments, such as trilobites, echinoderms, or brachiopods. Grain-rich parts of this facies are generally horizontally laminated. A total of 62 upward-fining cycles are recognised in the 75-cm-thick interval: 34 (55%) overlie lime mudstone (facies Lm), and 28 (45%) occur within shale. The lower boundary of this facies is usually sharp, and the overlying layer sometimes subangularly truncates more than two layers of the underlying facies (Fig. 5b). Facies Sg gradually fines upward and changes into parallel-laminated shale (facies Sl), or is directly overlain by lime mudstone (facies Lm) or bioclastic–intraclastic packstone-to-conglomerate (facies Cg) with diffuse to sharp upper contacts. Differential compaction features are common, which extend into overlying lime mudstone beds/nodules (Figs. 5a, b, and 6f). Bioturbation is absent in this facies.

Interpretation The sharp underlying boundaries and normal grading of this facies collectively suggest that decelerating flows such as storm-generated bottom currents or the distal regions of low-density turbidity currents were responsible for its formation (Kreisa 1981; Aigner 1982; Sepkoski et al. 1991; Zhou et al. 2011). The well-preserved primary lamination and absence of bioturbation indicate that the conditions were unfavourable for infauna, implying anoxic to dysoxic conditions (Hips 1998; Łabaj and Pratt 2016), or that the shale deposition was rapid. The compaction features would have resulted from differential loading during early diagenesis.

Parallel-laminated shale (facies Sl)

Description The parallel-laminated shale facies consists of dark grey mud-sized particles with some fossil fragments (Fig. 5c). Many mud-sized particles, and some larger fossil fragments, are aligned horizontally-to-subhorizontally and form laminations, which are generally parallel to the adjacent lime mudstone beds or nodules (Fig. 5d, e). Borings and burrows, which is observed in lime mudstone (facies Lm), is notably absent. A gradual transition from the underlying coarser-grained facies (facies Sg) to this facies was often observed (Fig. 5). Very thin (less than a few grains thick) bioclastic laminae with erosive lower boundaries sporadically occurs within the parallel-laminated shale facies, possibly corresponding to the basal calcarenite unit of normally graded shale facies (Fig. 5c, e). When this facies experiences compaction, it may resemble normally graded shale (facies Sg) (Fig. 5a).

Interpretation Parallel lamination of shale could have been formed by suspension and settling of hemipelagic siliciclastic sediments or lower/upper-flow-regime currents that were supplied by various processes such as buoyant plumes,

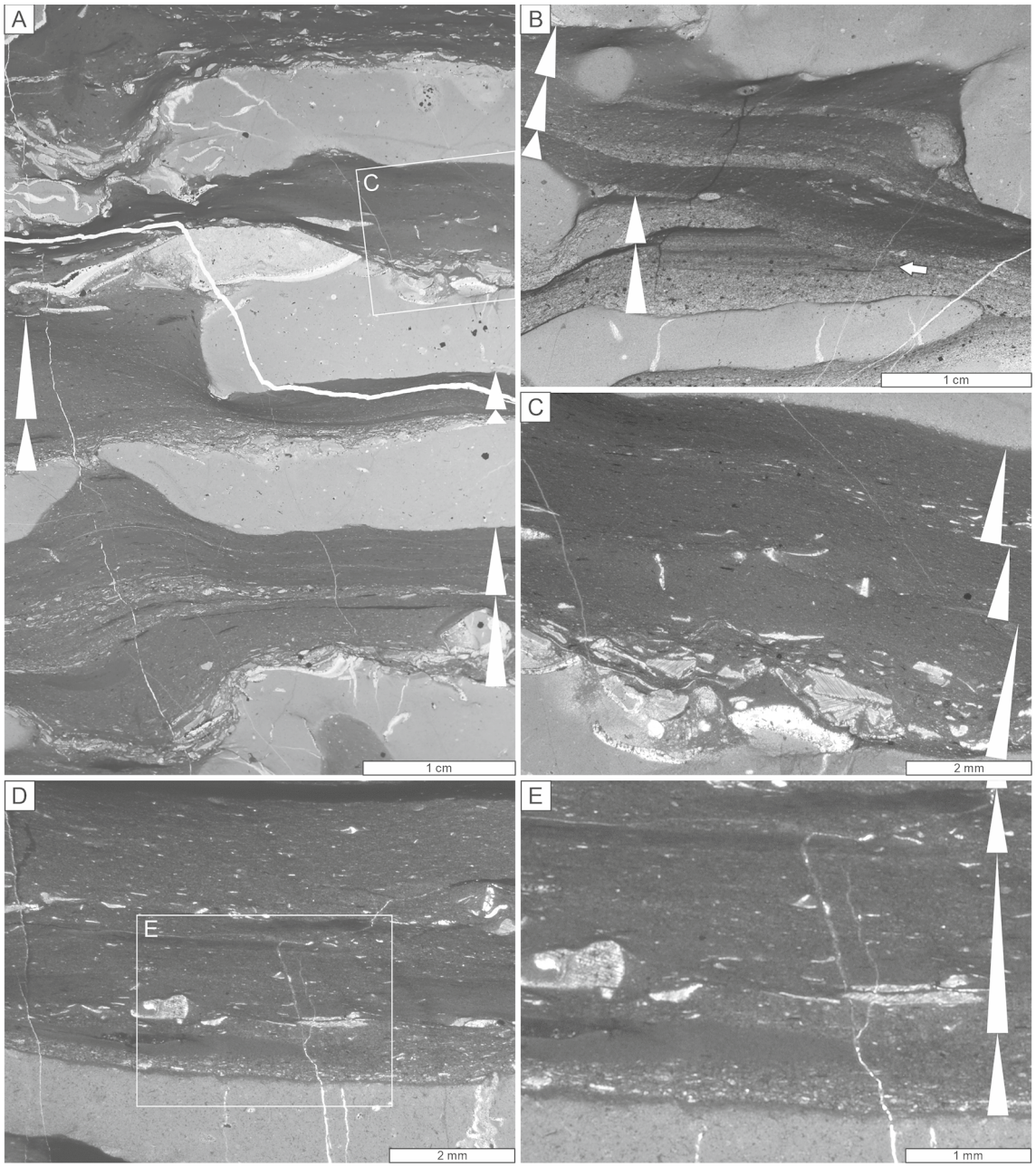

Fig. 5 Photomicrographs of the shale (facies Sg, Sl). Fining-upward cycles within the shale are marked with white triangles. **a** Photomicrograph of the ribbon rock. Shale beds are intercalated between lime mudstone. Differential compaction has often caused lateral variability in shale thickness. **b** Normally graded calcarenite to shale, truncating underlying deposits (arrow). **c** Close-up of **a**. Note the occurrence of three cyclic changes from underlying normally graded calcarenite to shale to overlying parallel-laminated shale. **d** Alternations of normally graded calcarenite to shale and parallel-laminated shale. **e** Close-up of **d**. Very thin bioclastic laminae with erosive boundary can be recognised at the base of some parallel-laminated shale layers

gravity flows, and unidirectional currents driven by storms and tides (Markello and Read 1981; Moshier 1986; O'Brien 1990, 1996; Southard and Boguchwal 1990; Aplin and Macquaker 2011; Lazar et al. 2015). Bioclasts within the shale could have been re-oriented during the compaction process (Lash and Blood 2004; Aplin et al. 2006). However, the parallel lamination could have been modified from low-angle cross lamination; as proven by experimental studies, cross-laminae can become oriented parallel to bedding after compaction (Schieber and Yawar 2009; Trabucho-Alexandre et al. 2012; Egenhoff and Fishman 2013). The frequent occurrence of thin bioclastic laminae at the base of this facies and the occurrence of sharp bases suggest that, overall, the facies may represent deposits of non-turbulent

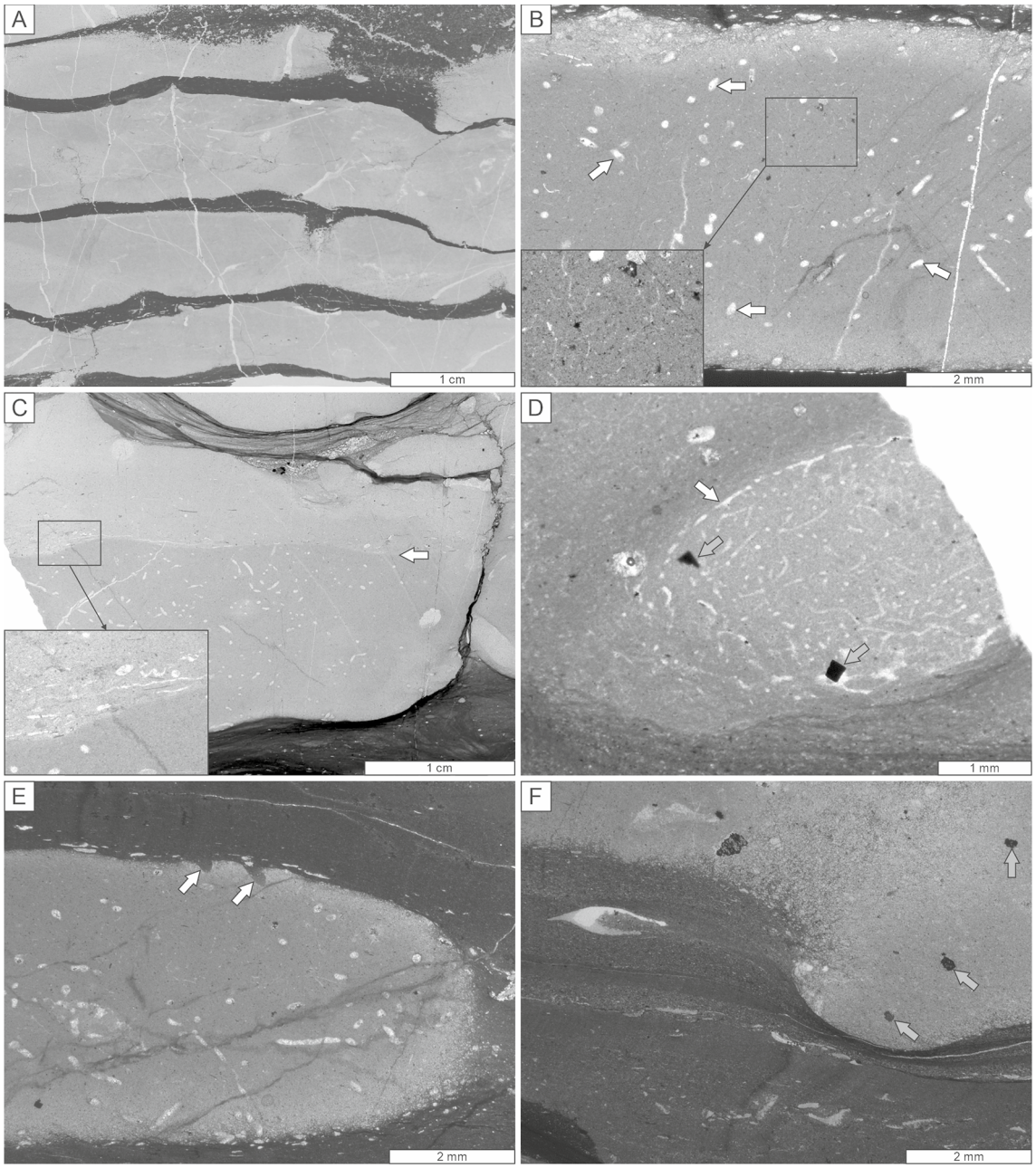

Fig. 6 Photomicrographs of the lime mudstone (facies Lm). **a** Thin bedded lime mudstone interbedded with shale. **b** Lime mudstone with poorly preserved vermiform fabrics (calcified remains of keratose sponge). This facies contains abundant microborings (arrowed) filled with cement. Lower left shows details of the facies. **c** Homogeneous lime mudstone overlying lime mudstone with microborings. Note the occurrence of a sharp boundary (arrow) between these two lime mudstones and the presence of tiny bioclastic fragments above the boundary (enlarged at lower left). **d** A relatively well-preserved example of vermiform fabric (keratose sponge), with a clear margin (white arrow). Euhedral pyrite crystals (grey arrows) can be observed in the vermiform fabric. Sample from the Hyeoldong section (37°08′02″ N, 128°55′10″ E). **e** Nodular lime mudstone. The nodule has a diffuse right margin and borings on the upper surface (arrows). **f** The lower boundary of facies Lm. On the right side, well-lithified lime mudstone with a sharp margin is pressed into the underlying shale. Partly or non-lithified lime mudstone on the left side is bounded by a diffuse boundary. Arrows indicate pyrite crystals

lower-energy flows that arose from storm bottom currents (Einsele 1998). Such weakly graded, laminated structures are common in modern storm deposits (Reineck and Singh 1972; Kreisa 1981; Sepkoski et al. 1991). The upper part of the facies may represent hemipelagic siliciclastic sediments supplied during fair-weather periods. The absence of bioturbation suggests dysoxic to anoxic conditions (Łabaj and Pratt 2016).

Lime mudstone (facies Lm)

Description The lime mudstone facies is the dominant type of limestone in the couplets and exhibits variable shapes, from horizontally extended thin layers (Fig. 6a) to circular to elliptical nodules 2–12 mm thick (Fig. 6e). This facies is mostly composed of micrite, with rare bioclastic fragments (trilobites, echinoderms, and brachiopods) (Fig. 6c) and euhedral pyrite crystals (Fig. 6d, f). Borings and burrows (up to 4 mm wide) are often present within the studied interval (Fig. 6b, c, e). Two types of borings are described: variously directed tube-shaped microborings (110–160 μm diameter, maximum length 2 mm) that are filled with sparite (Fig. 6b) and minor tube-shaped *Trypanites* (maximum diameter 0.5 mm) (Fig. 6e). There are no recognisable sedimentary structures within this facies, except for the burrows/borings and rare erosive surfaces (Fig. 6c). The boundaries of the limestone nodules/layers are sharp to diffuse. Some sharp upper boundaries form an erosional surface with the overlying facies Sg and Sl. In some cases of diffuse boundaries, micrite grades into microspar at the margin of the nodule and calcite crystals are dispersed in the surrounding shale (Fig. 6e, f). Locally, vermiform fabrics resulted from calcified remains of keratose sponges (Luo and Reitner 2014) were recognised (six of 52 limestone–shale couplets; 11%) comprising relatively regular networks of curved microsparfilled tubules that are ca. 10 μm wide and up to 200 μm long (Fig. 6b, d). The vermiform fabrics rarely show well-defined margins (Fig. 6d), similar to an Upper Ordovician example from South China (Park et al. 2015, Fig. 6d).

Interpretation As there are no sedimentary structures within this facies that provide evidence for its formation process, it is not possible to clarify origin of the micrite. The occurrence of sharp, erosional boundaries on top of these nodules as well as borings/burrows suggest that, regardless of the micrite origin, the facies was exposed at the sediment–water interface before the deposition of subsequent layers, and possibly during primary deposition as well (Kennedy and Garrison 1975; Möller and Kvingan 1988). The lime mudstones would have experienced early cementation because of favourable sea-water chemistry (i.e., calcite seas) (Wilson et al. 1992; Kim and Lee 1996; Lee et al. 2015; Wright and Cherns 2016b) and elevated sea-water temperature (Trotter et al. 2008; Elrick et al. 2011; Goldberg et al. 2021) while the intercalated shale facies (facies Sg and Sl) remained unlithified. During early burial, the unlithified, liquefied shale would undergo mechanical compaction and dewatering (see facies Sg). This process might have broken the partially lithified thin-bedded limestone and formed nodules.

Three possible scenarios are proposed: hemipelagic suspension settling of micrite; transportation by mudflow; or early diagenetic segregation within calcareous mudstone (e.g., Coniglio and James 1990). If the micrites had been formed by primary sedimentary processes, they would have been generated in the shallower platform by organisms or in the shallow water column by inorganic precipitation of whitings (Shinn et al. 1989; Morse et al. 2003). The absence of calcifying plankton in the early Palaeozoic ocean negates the possibility of a pelagic organic origin (Eichenseer et al. 2019). Syndepositional bacterial degradation of sponge soft tissue (Reitner 1993; Warnke 1995; Luo and Reitner 2014) could have been responsible for the formation of vermiform micrites (Park et al. 2015; Lee and Riding 2021), although detailed analysis may be nessary to confirm origin of the vermiform fabrics (Kershaw et al. 2021). Some of the micrites, especially those containing fossil fragments and with sharp bases, are likely to have formed by mudflows (Fig. 6c), although such examples occur only rarely in the study interval. The spherical to ellipsoidal shapes of some nodules and the diffuse contact with increased crystal size toward the margin may indicate early diagenetic growth of concretions for some micrites (Hallam 1986; Möller and Kvingan 1988; Arzani 2006; Westphal et al. 2008). In such a case, diagenetic growth of nodules would have occurred during very shallow burial, a few centimetres to decimetres below the sediment–water interface, as the nodules would have been exposed above the seafloor and experienced erosion (Möller and Kvingan 1988). However, the absence of primary sedimentary structures (e.g., laminations) that laterally extend from the adjacent shale into the nodules suggests that such diagenetically formed nodules may be uncommon in Hwajeol examples, although some ellipsoidal nodules with diffuse margins could have been solely formed by diagenesis. Some primary lime mudstone could have been modified by diagenetic growth, but it is not currently possible to distinguish between these possibilities.

Wackestone-to-packstone (facies WP)

Description The wackestone-to-packstone facies is characterised by micritic clasts and skeletal grains supported by a micritic matrix (Fig. 7b). Clasts are generally well-rounded with relatively low sphericity, ranging from coarse sand to gravel size. Trilobite and echinoderm fragments often occur within this facies. The lower boundary of this facies is usually sharp and flat, and truncates underlying facies such as lime mudstone or shale (Fig. 7b). In contrast, the upper boundary of this facies is often undulatory, formed along the margin of clasts within the facies, or truncated by overlying shale (facies Sg and Sl) or grainstone (facies Cg) facies.

Interpretation Micritic clasts would have originated from the erosion of underlying lime mudstone substrates (facies Lm) that had experienced submarine lithification, either at

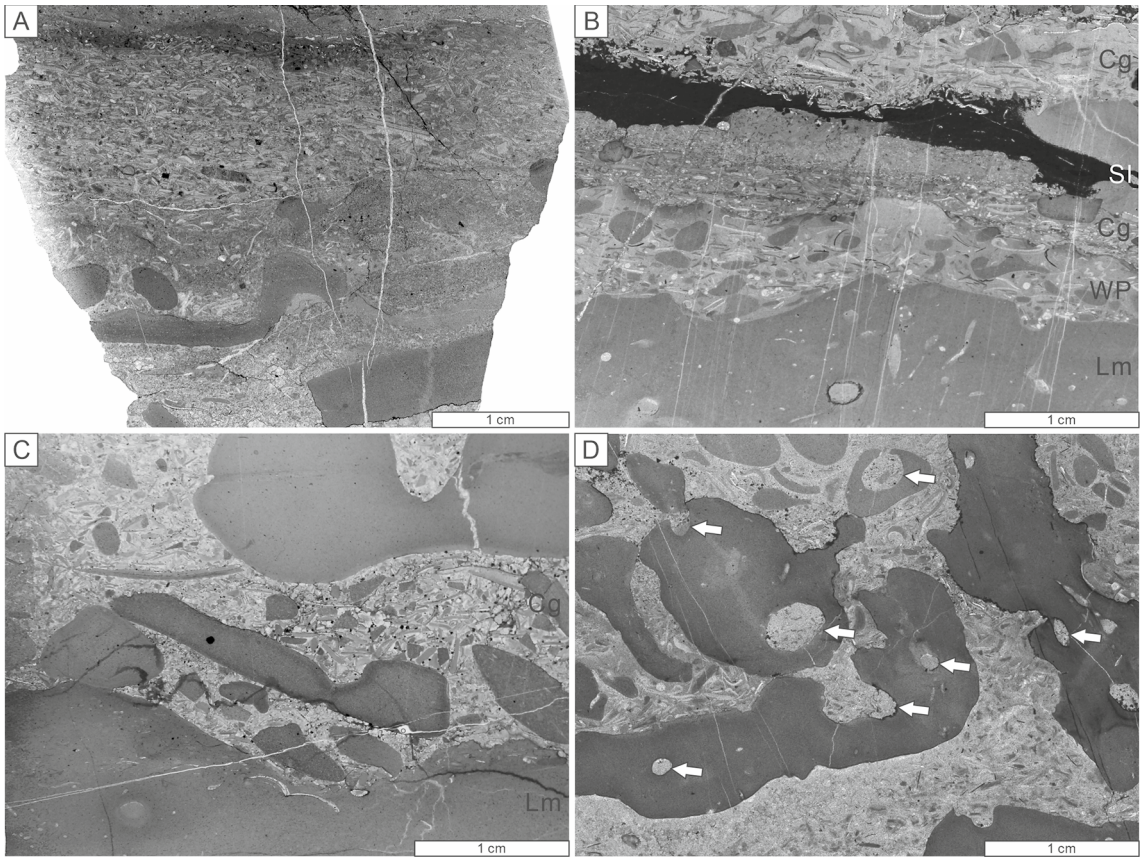

Fig. 7 Photomicrographs of wackestone-to-packstone (facies WP) and bioclastic–intraclastic packstone-to-conglomerate (facies Cg). **a** Flat-pebble conglomerate with a grainstone matrix gradually changing upward into a skeletal grainstone. **b** Micritic matrix-supported packstone-to-conglomerate truncating underlying lime mudstone (facies Lm). The packstone is truncated by the overlying skeletal grainstone. Sl; parallel-laminated shale. **c** Flat-pebble conglomerate with grainstone matrix, sharply truncating underlying lime mudstone with a few bioclasts. **d** Macroborings (arrows) within micritic clasts of flat-pebble conglomerates. Photomicrograph after Lee et al. (2018)

the sea floor or within the very shallow subsurface (Myrow et al. 2004; Wright and Cherns 2016b). The sharp lower boundary and poorly sorted nature of the facies collectively indicate that the components of this facies were transported together by mudflows (Shanmugam and Benedict 1978; Sawyer et al. 2012).

Bioclastic–intraclastic packstone-to-conglomerate (facies Cg)

Description The bioclastic–intraclastic packstone-to-conglomerate facies is characterised by well-rounded flat-pebble intraclasts with low sphericity that are embedded within a bioclastic packstone-to-grainstone matrix composed of trilobite and echinoderm fragments (Fig. 7). This facies forms the thickest beds in the entire study interval, and is commonly a few centimetres to decimetres thick. The conglomerate is generally clast-supported, and displays some imbrication (Fig. 4f). The texture of this facies sometimes changes vertically (Fig. 7a). In some cases, the lower part of the facies contains abundant intraclasts, which grades upward into grainstone texture without clasts. In other cases, the lower part exhibits grainstone texture; whereas, the upper part has packstone texture. Most of the clasts are composed of pure micrite, although some bioclastic wackestone, peloidal packstone, and multi-generation clasts occur. Some of the intraclasts were bored during or before the formation of intraclasts, with *Trypanites* and *Gastrochaenolites*-like borings (Fig. 7d) (Lee et al. 2018). The lower boundary of this facies is sharp (Fig. 7c).

Interpretation The polymictic intraclasts and sharp lower boundary indicate that the components of this facies were transported by flow events (Demicco and Hardie 1994; Pratt and Bordonaro 2007). Micritic clasts would have become horizontally and subhorizontally aligned by strong currents, similar to other flat-pebble conglomerates of this time (Sepkoski 1982; Demicco and Hardie 1994; Myrow et al. 2004). The packstone texture occurring in the lower part can be interpreted as resulting from gravity flows such as debris

flows (Shanmugam and Benedict 1978; Sawyer et al. 2012). Given the predominance of mud-sized sediment in the study interval, it is also possible that after deposition of the facies, micrite settled and infiltrated between intraclasts at the top (Reid et al. 1990). The components of intraclasts are generally similar to those in the nearby micritic limestones, suggesting that these intraclasts originated from a local source (Pohler and James 1989; Belka et al. 1996). On the other hand, bioclasts would have originated from the shallower part of the carbonate platform (Myrow et al. 2004).

Facies distribution in the Hwajeol ribbon rock

In the Hwajeol ribbon rock, lime mudstone (facies Lm; 46.7% of thin-section area) and shale facies (facies Sg and Sl; 34.8% of thin-section area) are the most common facies, whereas, coarser sediments (wackestone–packstone (facies WP) and grainstone (facies Cg); 1.6% and 16.9% of thin-section area, respectively) are less abundant in the 75-cm-thick interval (Fig. 3). Among the 96 lime mudstone nodules to layers, the majority (89 of 96; 93%) of them overlie parallel-laminated shale, but some occur on top of normally graded calcarenite to shale (five of 96; 5%) or bioclastic–intraclastic packstone (two of 96; 2%). These lime mudstone nodules to layers are overlain by normally graded calcarenite to shale (46 of 96; 48%), parallel-laminated shale (42 of 96; 44%), wackestone–packstone (four of 96; 4%) or bioclastic–intraclastic packstone to grainstone (three of 96; 3%). Wackestone–packstone (facies WP) is generally uncommon, mostly overlies lime mudstone and is overlain by parallel-laminated shale (eight of nine; 89%), and only one example occurs within the normally graded calcarenite to shale (one of 9; 11%). Only four beds of conglomerate (facies Cg) were described from the 75-cm-thick interval. Upward-fining cycles of shales (from facies Sg to Sl) are very abundant (62 boundaries) within the 75-cm-thick interval.

Discussion

Formative process of the Hwajeol ribbon rock

The formative process of the Hwajeol ribbon rock in the studied interval can be summarised as follows. The micritic sediments are likely to have formed by hemipelagic settling of lime mud and minor mudflows supplied from the nearby shallow carbonate platform or at least partly by keratose sponges, and then burrowed. Early diagenetic formation of concretions below the sediment–water interface within the siliciclastic mud cannot be fully discarded. These micritic sediments then experienced submarine lithification, either at the sea floor or within the sediment. The lithified lime mudstone consequently exposed at the sediment–water interface, where they got eroded and bored. Storm-induced bottom currents would have truncated the lime mudstones and/or deposited shale. The occurrence of numerous erosive surfaces and upward-fining cycles suggests that each cycle reflects repetitive short-term-scale storm events. Differential compaction and subsequent soft-sediment deformation of lime mudstone and shale would have resulted in nodular limestone. Conglomerate beds may represent events occurring on a scale of ten thousand to hundreds of thousand years such as mega-storms, tsunamis, or earthquakes (Myrow et al. 2004; Pratt and Bordonaro 2007). A similar storm-induced model was previously proposed for the ribbon rocks, but that model suggested that the carbonate sediments are storm deposits whereas the siliciclastic sediments are background deposits, in contrast to our model for the Hwajeol ribbon rocks (Markello and Read 1981; Sami and Desrochers 1992; Bayet-Goll et al. 2015). The current model thus presents a tempestite origin of Hwajeol-type ribbon rocks, and emphasises the importance of sedimentary structures preserved within the shale.

Types of ribbon rock

Ribbon rocks similar to that of the Hwajeol Formation are a common sedimentary facies of the lower Palaeozoic (Table 2). Although this rock type is commonly called "ribbon rock", at least four different types of ribbon rock have been defined: tempestite type (this study); tidalite type (e.g., Demicco 1983); turbidite type (e.g., Coniglio and James 1990); and diagenetic type (e.g., Westphal et al. 2000). The different types may occur in a range of environments, from supratidal to deep basin. For example, Bayet-Goll et al. (2015) demonstrated that the ribbon rock-dominated middle Cambrian platform of Iran contains various environments, ranging from intertidal to deep subtidal below storm wave base. The Iranian example demonstrates correct definition of lithofacies is important to reconstruct depositional environments during the early Palaeozoic. Below we compare the tempestite-type ribbon rocks of the Hwajeol Formation with other types of ribbon rocks and present criteria to distinguish different ribbon rock types.

Tempestite-type ribbon rocks can be differentiated from those formed in Cambrian tidal flats. Tidalite-type ribbon rocks are characterised by alternations of grainy sediment showing (bi-directional) cross-lamination and muddy sediment and are associated with intertidal to supratidal sedimentary structures such as mudcracks and microbial laminites (Demicco 1983; Chow and James 1987; Álvaro and Vennin 1997; Bayet-Goll et al. 2015; Zhang et al. 2015) (Fig. 8a). This type of rock is interpreted to have been formed by tidal currents, similar to flaser and lenticular bedding, based on the alternation of sediments of different grain

Table 2 Selected occurrences of limestone-shale couplet similar to that of the Hwajeol Formation

Location	Age	Formation	Facies name	Description	Interpretation	References
California, USA	Miaolingian	Carrara Fm	Ribbon rock	Alternation of 1–4 cm thick limestone (packstone, grainstone, and arenite/siltite) and ~ 1 cm thick dolostone; sedimentary structures generally absent except for some planar laminae, trough cross-beds, and ripples; bioturbation present	Subtidal environment in between fair-weather wave base and storm-wave base	Adams and Grotzinger (1996)
Nevada and Utah, USA	Miaolingian	Marjum Fm	Rhythmite	Alternation of laminated to massive pelleted microspar limestone and laminated argillaceous limestone beds; each couplet ranges 3–20 cm in thickness	Deposition in quite waters below and near storm wave base formed by suspension-settling or dilute density current; climatically controlled changes in terrigenous and/or detrital carbonate fluxes	Elrick and Snider (2002)
Iran	Miaolingian	Deh-Sufiyan Fm	Limestone and shale alternation	Intercalation of planar, partly wavy or nodular, lime mudstone–wackestone (homogeneous, partly cross- or parallel-lamination) and shale or dolomitic shale; weakly bioturbated	Low-energy deep subtidal environments below the storm wave base; frequent input of carbonates during background deposition of fine-grained siliciclastic sediment	Bayet-Goll et al. (2015)
Inner Mongolia, China	Miaolingian	Abuqiehai Fm	Interbedded lime mudstone and marlstone	0.2–5-cm-thick interbedded lime mudstone (tabular, undulatory, nodular, and irregular geometries, and diffuse and distinct boundaries) and dolomitic marlstone or calcareous shale; ball-and-pillow structures locally present; some beds are mildly bioturbated	Deposition from suspension in a low-energy setting; varying influence of sediment supply from both terrestrial and in situ marine sources	Myrow et al. (2015); Lee et al. (2016b)

Table 2 (continued)

Location	Age	Formation	Facies name	Description	Interpretation	References
Southwest Virginia-Tennessee, USA	Miaolingian–Furongian	Maryville, Nolichucky, and Maynardville fms	Ribbon limestone	Thin-bedded carbonate alternating with siltstone/shale; carbonate layers consist of skeletal grainstone or peloidal-skeletal wackestone/packstone-to-mudstone (horizontally laminated and burrowed); commonly fining upward	Deep-ramp below normal wave base by erosion and redeposition of sediments by storms (Markello and Read 1981, 1982; Srinivasan and Walker 1993; Rankey et al. 1994) or storm-dominated shallow ramp (Glumac and Walker 1997, 2000)	Markello and Read (1981, 1982); Srinivasan and Walker (1993); Rankey et al. (1994); Glumac and Walker (1997, 2000)
Shandong, China	Miaolingian–Furongian	Gushan and Chaomidian fms	Ribbon rock (limestone-shale couplet/alternation)	Alternation of planar to nodular micritic limestone and shale; sporadic horizontal burrows	Low-energy subtidal deposit below fair-weather wave base	Chen et al. (2009, 2010, 2011)
Newfoundland, Canada	Miaolingian–Furongian	Port au Port Group (March Point, Petit Jardin, and Berry Head fms.)	Parted limestone/ribbon rock	Lime mudstone beds (planar or lenticular; 2–10 cm thick) separated by shale beds (~ 1 cm or 2–10 cm thick); shale consists of alternating dark and light laminae	Grainy sediments: turbidites, shale: terrigenous turbidite (Bouma E), lime mudstone: diagenesis during shallow burial or deposition from turbidity currents or hemipelagic settling	Chow and James (1987, 1992); Coniglio and James (1990); Cowan and James (1992, 1993)
Taebaek, Korea	Furongian	Hwajeol Fm	Limestone-shale couplet	Alternation of ~ 2 cm thick micritic limestone and shale; limestone beds nodular to planar, some with sponge networks; grading and/or lamination within shale beds	Alternation of fair-weather deposit (micritic limestone) and gravity flow deposit induced by storm events (shale, grainstone, and conglomerate)	Kwon et al. (2006); Byun and Kwon (2020); This study
Pennsylvania, USA	Furongian	Richland Fm	Ribbon carbonate	Interlaminated "ribbons" of millimetre- to centimetre-thick micritic limestone and dolomitic mudstone	Deep subtidal deposits formed by fluctuating sediment input or flow regime	Moshier (1986)
Taebaek, Korea	Lower Ordovician	Dumugol Fm	Limestone-shale couplet	Alternation of planar or nodular lime mudstone and dolomitic shale layers	Distal storm deposits (limestone) and background deposits (shale) in ramp; cyclic pulses or lateral facies variations	Kwon and Chough (2005)

Table 2 (continued)

Location	Age	Formation	Facies name	Description	Interpretation	References
Virginia, USA	Lower Ordovician	Chepultepec and Stonehenge fms	Ribbon carbonate	Mud/wackestone or fine pellet grainstone with mud interlayer	Offshore open marine setting, quite-water subtidal facies; storm deposits	Bova and Read (1987)

sizes and the association with peritidal facies (Demicco 1983).

Turbidite-type ribbon rock is an important type of ribbon rock that occurs throughout the Cambrian–Ordovician platform margin sequence of Newfoundland, Canada (Coniglio and James 1990). The calcilutite/shale lithofacies of Coniglio and James (1990) has been interpreted to have been formed by partial diagenetic alteration of sediment from turbidity currents and/or hemipelagic settling, or entirely by diagenesis. Turbidite-type ribbon rocks are characterised by laterally traceable (> 10 s of metres) limestone and shale layers of even thickness, with partial Bouma sequences preserved in limestone layers (Fig. 8b), that can be distinguished from laterally discontinuous tempestite-type.

Differential diagenesis has been introduced to explain the origin of ribbon rock. According to this model, calcium carbonate migrates into the limestone layers from the marlstone interlayers during early diagenesis, resulting in cementation of the limestone prior to mechanical compaction. Evidence for this model is the existence of largely uncompacted limestone beds and intensely compacted interlayered marlstones, and laterally traceable sedimentary structures from the limestone to the adjacent marlstone layers (Westphal et al. 2000, 2008; Westphal 2006; Amberg et al. 2016; Nohl et al. 2019; Nohl and Munnecke 2019). These diagenetic-type ribbon rocks are markedly different from tempestite-type ribbon rocks, because they lack erosive surfaces along the limestone–shale boundaries (e.g., Westphal et al. 2008; Nohl et al. 2019). Diagenetic-type ribbon rocks are especially common in Jurassic and Cretaceous strata (Westphal et al. 2008), but are also found from other time intervals (Nohl et al. 2019).

In addition, climatically controlled change in carbonate and/or siliciclastic sediment input by suspension-settling or dilute density currents has been proposed for the origin of the ribbon rocks, which suggests they are rhythmites (Elrick and Snider 2002). Considering the thickness of the studied interval to the upper boundary of the Hwajeol Formation (~ 50 m) and duration (4–5 Myr), as well as the thickness of each thin-bedded or nodular shale and limestone (~ 1 cm), the approximate duration of each ribbon rock layer (~ 1 cm/1000 year) is too short to reflect Milankovitch cycles. Nonetheless, it will be necessary to discuss the detailed sedimentary processes of ribbon rocks prior to applying cyclostratigraphic interpretations.

Temporally restricted occurrences of Hwajeol-type ribbon rocks

The known occurrences of ribbon rocks similar to those of the Hwajeol Formation are mainly concentrated in middle Cambrian–Lower Ordovician successions worldwide (Table 2). Interestingly, flat-pebble conglomerates

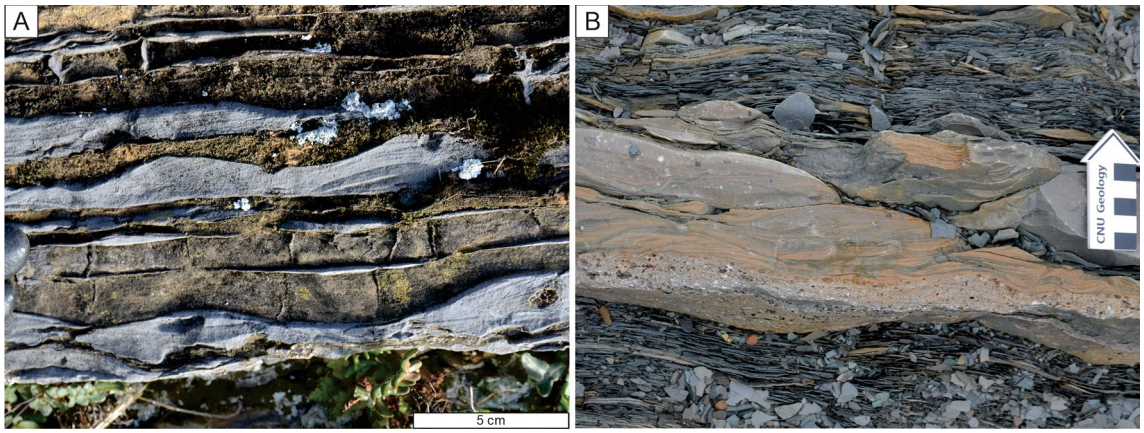

Fig. 8 Other types of ribbon rocks. **a** Wavy and lenticular-bedded ribbon rock of the Conococheague Limestone (upper Cambrian), exposed along the Chesapeake and Ohio Canal Towpath at Clear Spring, Maryland, USA (39°36′34″ N, 77°55′27″ W). Note cross-stratified calcarenite with flat base. See Demicco (1983) for formative processes. **b** Green Head Global Stratotype Section and Point, Newfoundland, Canada (uppermost Cambrian) (49°40′57″ N, 57°57′52″ W). An interbedded limestone layer shows a gradual fining-upward trend from gravelly calcirudite into cross-stratified calcarenite that can be interpreted as Ta to Tb of the Bouma sequence. Scale in centimetres. See Coniglio and James (1990) for formative processes

characterised by flat, rounded micritic clasts are also confined to coeval strata (Zhuravlev and Wood 2008; Wright and Cherns 2016b). The formation of flat-pebble conglomerates is thought to be closely linked with ribbon rocks (Sepkoski 1982; Myrow et al. 2004; Chen et al. 2009), because submarine lithification of micritic substrates to produce thin-bedded limestone is essential for the formation of the micritic intraclasts of flat-pebble conglomerates (Wright and Cherns 2016a, b). The limestone would have been reworked to form micritic intraclasts (Sepkoski 1982; Kim and Lee 1995; Myrow et al. 2004) or experienced soft-sediment deformation during early burial (Kwon et al. 2002; Chen et al. 2009). Understanding the formative mechanisms of the ribbon rock would thus provide a clue to solve the question of how this extraordinary sedimentary facies of the early Palaeozoic formed.

The occurrence of ribbon rock has been suggested to have been controlled by two major factors: sea-water chemistry inducing precipitation of calcite and the abundance of infauna (Sepkoski 1982). The aragonite sea of the Terreneuvian and Cambrian Series 2 transitioned into a calcite sea during the Miaolingian, which would have promoted precipitation of calcium carbonate, accompanied by elevated temperature in the later Cambrian (Zhuravlev and Wood 2008; Lee et al. 2015; Lee and Riding 2018). As a result, thin-bedded limestone could have been deposited between storm events as a background deposit. The resulting deposit could have been preserved unless biota living on the seafloor destroyed the sedimentary structure (Droser and Bottjer 1988), as happened in the later Palaeozoic and after. Prior to the Great Ordovician Biodiversification Event, when burrowers expanded to the deeper part of the ocean, deep-water sediments could have been preserved without disruption (Sepkoski 1982; Bottjer et al. 2000; Droser and Li 2001; Liu 2009; Buatois et al. 2016). The lower Palaeozoic ribbon rocks, therefore, preserve various sedimentary processes that occurred in the deeper part of the ocean during the calcite sea interval. These sediments could not have been preserved during the rest of the Phanerozoic (probably excluding those deposited during the post-mass extinction intervals and in the oxygen minimum zones), and thus provide a unique window to understand the sedimentary processes that operated in deep-water carbonate environments at that time.

Conclusions

This study documents the formative mechanism of ribbon rock from the Furongian Hwajeol Formation, Korea, which is characterised by the alternation of thin-bedded lime mudstone and shale. Shales, as well as intercalating flat-pebble conglomerates, were formed by storm-induced bottom currents as event deposits, whereas lime mudstones were formed as background deposits by suspension-settling of micritic sediment produced from the shallower part of the platform and/or the upper part of the water column, by sponges living on the seafloor, or by diagenetic concretions. Sporadic larger storm events would have transported and deposited coarser-grained grainstones and conglomerates. The Hwajeol ribbon rock is classified as a tempestite-type and can be distinguished from other types of ribbon rocks—tidalite, tempestite, and diagenetic types. The formation of the ribbon rocks was enhanced by the characteristic sea-water chemistry that enhanced carbonate precipitation and

the scarcity of burrowers during the early Palaeozoic. This study may provide a key to help understand the sedimentary processes in the deeper portions of Cambro–Ordovician carbonate platforms as well as during other periods of the Phanerozoic, for which sedimentary structures are not preserved as a result of the expansion of burrowing biota into deep environments.

Acknowledgements This study was supported by grants from the National Research Foundation of Korea to JHL (2019R1A2C4069278) and SJC (2018R1A2A2A05018469). We thank S.-W. Kwon for help with fieldwork and preparation of thin sections and sedimentary logs, and A. Munnecke, J. Wheeley and T. Nohl for their constructive comments. This study is a contribution to IGCP Project 735 "Rocks and the Rise of Ordovician Life: Filling knowledge gaps in the Early Palaeozoic Biodiversification".

Declarations

Conflict of interest The authors declare that they have no conflict of interest.

References

Adams RD, Grotzinger J (1996) Lateral continuity of facies and parasequences in middle Cambrian platform carbonates, Carrara Formation, southeastern California, U.S.A. J Sediment Res 66:1079–1090. https://doi.org/10.1306/D42684AF-2B26-11D7-8648000102C1865D

Aigner T (1982) Calcareous tempestites: storm-dominated stratification in upper Muschelkalk limestones (middle Trias, SW Germany). In: Einsele G, Seilacher A (eds) Cyclic event and stratification. Springer-Verlag, Berlin, pp 180–198

Álvaro JJ, Vennin E (1997) Episodic development of Cambrian eocrinoid-sponge meadows in the Iberian Chains (NE Spain). Facies 37:49–64. https://doi.org/10.1007/BF02537370

Amberg CE, Collart T, Salenbien W, Egger LM, Munnecke A, Nielsen AT, Monnet C, Hammer O, Vandenbroucke TR (2016) The nature of Ordovician limestone-marl alternations in the Oslo-Asker district (Norway): witnesses of primary glacio-eustasy or diagenetic rhythms? Sci Rep 6:18787. https://doi.org/10.1038/srep18787

Aplin AC, Macquaker JHS (2011) Mudstone diversity: origin and implications for source, seal, and reservoir properties in petroleum systems. AAPG Bull 95:2031–2059. https://doi.org/10.1306/03281110162

Aplin AC, Matenaar IF, McCarty DK, van der Pluijm BA (2006) Influence of mechanical compaction and clay mineral diagenesis on the microfabric and pore-scale properties of deep-water Gulf of Mexico mudstones. Clays Clay Miner 54:500–514. https://doi.org/10.1346/CCMN.2006.0540411

Arzani N (2006) Primary versus diagenetic bedding in the limestone-marl/shale alternations of the epeiric seas, an example from the lower Lias (early Jurassic) of SW Britain. Carbonates Evaporites 21:94–109. https://doi.org/10.1007/BF03175469

Bayet-Goll A, Chen J, Moussavi-Harami R, Mahboubi A (2015) Depositional processes of ribbon carbonates in middle Cambrian of Iran (Deh-Sufiyan Formation, central Alborz). Facies 61:9. https://doi.org/10.1007/s10347-015-0436-6

Belka Z, Skompski S, Sobon-Podgorska J (1996) Reconstruction of a lost carbonate platform on the shelf of Fennosarmatia: evidence from Viséan polymictic debrites, Holy Cross Mountains, Poland. In: Strogen P, Somerville ID, Jones GL (eds) Recent advances in lower Carboniferous geology. Geological Society of London special publications, vol 107. Geological Society of London, London, pp 315–329. https://doi.org/10.1144/GSL.SP.1996.107.01.22

Bottjer DJ, Hagadorn JW, Dornbos SQ (2000) The Cambrian substrate revolution. GSA Today 10:1–7

Bova JA, Read JF (1987) Incipiently drowned facies within a cyclic peritidal ramp sequence, Early Ordovician Chepultepec interval, Virginia Appalachians. Geol Soc Am Bull 98:714–727. https://doi.org/10.1130/0016-7606(1987)98%3c714:IDFWAC%3e2.0.CO;2

Buatois LA, Mangano MG, Olea RA, Wilson MA (2016) Decoupled evolution of soft and hard substrate communities during the Cambrian explosion and Great Ordovician Biodiversification Event. Proc Natl Acad Sci 113:6945–6948. https://doi.org/10.1073/pnas.1523087113

Byun UH, Kwon YK (2020) Depositional origin of subtidal meter-scale cyclic successions in the Cambrian Hwajeol Formation. Geosci J 24:1–16. https://doi.org/10.1007/s12303-018-0085-1

Chen J, Chough SK, Chun SS, Han Z (2009) Limestone pseudoconglomerates in the Late Cambrian Gushan and Chaomidian Formations (Shandong Province, China): soft-sediment deformation induced by storm-wave loading. Sedimentology 56:1174–1195. https://doi.org/10.1111/j.1365-3091.2008.01028.x

Chen J, Han Z, Zhang X, Fan A, Yang R (2010) Early diagenetic deformation structures of the Furongian ribbon rocks in Shandong Province of China—a new perspective of the genesis of limestone conglomerates. Sci China Earth Sci 53:241–252. https://doi.org/10.1007/s11430-010-0010-6

Chen J, Chough SK, Han Z, Lee J-H (2011) An extensive erosion surface of a strongly deformed limestone bed in the Gushan and Chaomidian Formations (late middle Cambrian to Furongian), Shandong Province, China: sequence–stratigraphic implications. Sediment Geol 233:129–149. https://doi.org/10.1016/j.sedgeo.2010.11.002

Cheong CH (1969) Stratigraphy and paleontology of the Samcheog Coalfield, Gangweondo, Korea (I). J Geol Soc Korea 5:13–56

Choi DK, Chough SK, Kwon YK, Lee SB, Woo J, Kang I, Lee HS, Lee SM, Sohn JW, Shinn YJ, Lee DJ (2004) Taebaek Group (Cambrian-Ordovician) in the Seokgaejae section, Taebaeksan Basin: a refined lower Paleozoic stratigraphy in Korea. Geosci J 8:125–151. https://doi.org/10.1007/BF02910190

Chough SK (2013) Geology and sedimentology of Korean Peninsula. Elsevier insights. Elsevier. https://doi.org/10.1016/C2012-0-02847-5

Chow N, James NP (1987) Cambrian grand cycles: a northern Appalachian perspective. Geol Soc Am Bull 98:418–429. https://doi.org/10.1130/0016-7606(1987)98%3c418:CGCANA%3e2.0.CO;2

Chow N, James NP (1992) Synsedimentary diagenesis of Cambrian peritidal carbonates: evidence from hardgrounds and surface paleokarst in the Port au Port Group, western Newfoundland. Bull Can Pet Geol 40:115–127. https://doi.org/10.35767/gscpgbull.40.2.115

Coniglio M, James NP (1990) Origin of fine-grained carbonate and siliciclastic sediments in an early Palaeozoic slope sequence, Cow Head Group, western Newfoundland. Sedimentology 37:215–230. https://doi.org/10.1111/j.1365-3091.1990.tb00956.x

Cook HE, Taylor ME (1977) Comparison of continental slope and shelf environments in the upper Cambrian and lowest Ordovician of Nevada. In: Cook HE, Enas P (eds) Deep-water carbonate environments. SEPM special publication, vol 25. SEPM, Tulsa, pp 51–81

Cowan CA, James NP (1992) Diastasis cracks: mechanically generated synaeresis-like cracks in upper Cambrian shallow water oolite and ribbon carbonates. Sedimentology 39:1101–1118. https://doi.org/10.1111/j.1365-3091.1992.tb01999.x

Cowan CA, James NP (1993) The interactions of sea-level change, terrigenous-sediment influx, and carbonate productivity as controls on upper Cambrian grand cycles of western Newfoundland, Canada. Geol Soc Am Bull 105:1576–1590. https://doi.org/10.1130/0016-7606(1993)105%3c1576:tioslc%3e2.3.co;2

Demicco RV (1983) Wavy and lenticular-bedded carbonate ribbon rocks of the upper Cambrian Conococheague Limestone, central Appalachians. J Sediment Petrol 53:1121–1132. https://doi.org/10.1306/212F8328-2B24-11D7-8648000102C1865D

Demicco RV, Hardie LA (1994) Sedimentary structures and early diagenetic features of shallow marine carbonates. SEPM atlas series, vol 1. SEPM, Tulsa

Droser ML, Bottjer DJ (1988) Trends in depth and extent of bioturbation in Cambrian carbonate marine environments, western United States. Geology 16:233–236. https://doi.org/10.1130/0091-7613(1988)016%3c0233:TIDAEO%3e2.3.CO;2

Droser ML, Li X (2001) The Cambrian radiation and the diversification of sedimentary fabrics. In: Zhuravlev AY, Riding R (eds) Ecology of the Cambrian radiation. Columbia University Press, New York, pp 137–169

Egenhoff SO, Fishman NS (2013) Traces in the dark—sedimentary processes and facies gradients in the upper shale member of the upper Devonian-lower Mississippian Bakken Formation, Williston Basin, North Dakota, U.S.A. J Sediment Res 83:803–824. https://doi.org/10.2110/jsr.2013.60

Eichenseer K, Balthasar U, Smart CW, Stander J, Haaga KA, Kiessling W (2019) Jurassic shift from abiotic to biotic control on marine ecological success. Nat Geosci 12:638–642. https://doi.org/10.1038/s41561-019-0392-9

Einsele G (1998) Event stratigraphy: recognition and interpretation of sedimentary event horizons. In: Doyle P, Bennett MR (eds) Unlocking the stratigraphical record: advances in modern stratigraphy. Wiley, New York, pp 145–193

Elrick M, Snider AC (2002) Deep-water stratigraphic cyclicity and carbonate mud mound development in the middle Cambrian Marjum Formation, House Range, Utah, USA. Sedimentology 49:1021–1047. https://doi.org/10.1046/j.1365-3091.2002.00488.x

Elrick M, Rieboldt S, Saltzman M, McKay RM (2011) Oxygen-isotope trends and seawater temperature changes across the late Cambrian Steptoean positive carbon-isotope excursion (SPICE event). Geology 39:987–990. https://doi.org/10.1130/g32109.1

Flügel E (2004) Microfacies of carbonate rocks: analysis, interpretation and application. Springer, Berlin

Glumac B, Walker KR (1997) Selective dolomitization of Cambrian microbial carbonate deposits: a key to mechanisms and environments of origin. Palaios 12:98–110. https://doi.org/10.2307/3515300

Glumac B, Walker KR (2000) Carbonate deposition and sequence stratigraphy of the terminal Cambrian grand cycle in the southern Appalachians, U.S.A. J Sediment Res 70:952–963. https://doi.org/10.1306/2dc40943-0e47-11d7-8643000102c1865d

Goldberg SL, Present TM, Finnegan S, Bergmann KD (2021) A high-resolution record of early Paleozoic climate. Proc Natl Acad Sci 118:e2013083118. https://doi.org/10.1073/pnas.2013083118

Hallam A (1986) Origin of minor limestone-shale cycles: climatically induced or diagenetic? Geology 14:609–612

Hips K (1998) Lower Triassic storm-dominated ramp sequence in northern Hungary: an example of evolution from homoclinal through distally steepened ramp to middle Triassic flat-topped platform. In: Wright VP, Burchette TP (eds) Carbonate ramps. Geological Society of London special publications, vol 149. Geological Society of London, London, pp 315–338. https://doi.org/10.1144/GSL.SP.1999.149.01.15

Jeong H, Lee YI (2000) Late Cambrian biogeography: conodont bioprovinces from Korea. Palaeogeogr Palaeoclimatol Palaeoecol 162:119–136. https://doi.org/10.1016/S0031-0182(00)00108-5

Kennedy WJ, Garrison RE (1975) Morphology and genesis of nodular chalks and hardgrounds in the upper Cretaceous of southern England. Sedimentology 22:311–386. https://doi.org/10.1111/j.1365-3091.1975.tb01637.x

Kershaw S, Li Q, Li Y (2021) Addressing a Phanerozoic carbonate facies conundrum—sponges or clotted micrite? Evidence from early Silurian reefs, south China Block. Sediment Rec 19:3–10. https://doi.org/10.2110/sedred.2021.1.03

Kim JC, Lee YI (1995) Flat-pebble conglomerate: a characteristic lithology of upper Cambrian and lower Ordovician shallow-water carbonate sequence. In: Cooper JD, Droser ML, Finney SC (eds) Ordovician Odyssey. Special publication, vol 77. SEPM Pacific Section, Fullerton, pp 371–374

Kim JC, Lee YI (1996) Marine diagenesis of lower Ordovician carbonate sediments (Dumugol Formation), Korea: cementation in a calcite sea. Sediment Geol 105:241–257. https://doi.org/10.1016/0037-0738(95)00141-7

Kobayashi T (1966) The Cambro-Ordovician formations and faunas of south Korea, part X, Stratigraphy of the Chosen Group in Korean and South Manchuria and its relation to the Cambro-Ordovician formations of other areas, section A. The Chosen Group of South Korea. J. Fac. Sci., Univ. Tokyo, Sect. II 16:1–84

Kreisa RD (1981) Storm-generated sedimentary structures in subtidal marine facies with examples from the middle and upper Ordovician of southwestern Virginia. J Sediment Petrol 51:823–848. https://doi.org/10.1306/212F7DBF-2B24-11D7-8648000102C1865D

Kwon YK, Chough SK (2005) Sequence stratigraphy of the cyclic successions in the Dumugol Formation (lower Ordovician), mideast Korea. Geosci J 9:305–324. https://doi.org/10.1007/BF02910319

Kwon YK, Chough SK, Choi DK, Lee DJ (2002) Origin of limestone conglomerates in the Choson Supergroup (Cambro-Ordovician), mid-east Korea. Sediment Geol 146:265–283. https://doi.org/10.1016/s0037-0738(01)00128-2

Kwon YK, Chough SK, Choi DK, Lee DJ (2006) Sequence stratigraphy of the Taebaek Group (Cambrian-Ordovician), mideast Korea. Sediment Geol 192:19–55. https://doi.org/10.1016/j.sedgeo.2006.03.024

Łabaj MA, Pratt BR (2016) Depositional dynamics in a mixed carbonate–siliciclastic system: middle-upper Cambrian Abrigo Formation, Southeastern Arizona, U.S.A. J Sediment Res 86:11–37. https://doi.org/10.2110/jsr.2015.96

Lash GG, Blood D (2004) Geochemical and textural evidence for early (shallow) diagenetic growth of stratigraphically confined carbonate concretions, upper Devonian Rhinestreet black shale, western New York. Chem Geol 206:407–424. https://doi.org/10.1016/j.chemgeo.2003.12.017

Lazar OR, Bohacs KM, Macquaker JHS, Schieber J, Demko TM (2015) Capturing key attributes of fine-grained sedimentary rocks in outcrops, cores, and thin sections: nomenclature and description guidelines. J Sediment Res 85:230–246. https://doi.org/10.2110/jsr.2015.11

Lee B-S (2014) Conodonts from the Sesong Slate and Hwajeol Formation (Guzhangian to Furongian) in the Taebaeksan Basin, Korea. Acta Geol Sin 88:35–45. https://doi.org/10.1111/1755-6724.12181

Lee J-H, Riding R (2018) Marine oxygenation, lithistid sponges, and the early history of Paleozoic skeletal reefs. Earth Sci Rev 181:98–121. https://doi.org/10.1016/j.earscirev.2018.04.003

Lee J-H, Riding R (2021) Keratolite–stromatolite consortia mimic domical and branched columnar stromatolites. Palaeogeogr

Palaeoclimatol Palaeoecol 571:110288. https://doi.org/10.1016/j.palaeo.2021.110288
Lee B-S, Seo K-S (2008) Conodonts from the Hwajeol Formation (upper Cambrian) in the Seokgaejae area, southeast margin of the Taebaeksan Basin. Geosci J 12:233–242. https://doi.org/10.1007/s12303-008-0024-7
Lee J-H, Chen J, Woo J (2015) The earliest Phanerozoic carbonate hardground (Cambrian stage 5, series 3): Implications to the paleoseawater chemistry and early adaptation of hardground fauna. Palaeogeogr Palaeoclimatol Palaeoecol 440:172–179. https://doi.org/10.1016/j.palaeo.2015.07.043
Lee J-H, Hong J, Woo J, Oh J-R, Lee D-J, Choh S-J (2016a) Reefs in the early Paleozoic Taebaek Group, Korea: a review. Acta Geol Sin 90:352–367. https://doi.org/10.1111/1755-6724.12659
Lee J-H, Kim B-J, Liang K, Park T-Y, Choh S-J, Lee D-J, Woo J (2016b) Cambrian reefs in the western north China platform, Wuhai, inner Mongolia. Acta Geol Sin 90:1946–1954. https://doi.org/10.1111/1755-6724.1301410.1111/1755-6724.13014
Lee J-H, Choh S-J, Lee D-J (2018) Late Cambrian missing link in macroborer evolution preserved in intraclasts. Palaeogeogr Palaeoclimatol Palaeoecol 489:137–146. https://doi.org/10.1016/j.palaeo.2017.10.005
Liu J (2009) Marine sedimentary response to the Great Ordovician Biodiversification Event: examples from north China and south China. Paleontol Res 13:9–21. https://doi.org/10.2517/1342-8144-13.1.009
Luo C, Reitner J (2014) First report of fossil "keratose" demosponges in Phanerozoic carbonates: preservation and 3-D reconstruction. Naturwissenschaften 101:467–477. https://doi.org/10.1007/s00114-014-1176-0
Markello JR, Read JF (1981) Carbonate ramp-to-deeper shale shelf transitions of an upper Cambrian intrashelf basin, Nolichucky Formation, southwest Virginia Appalachians. Sedimentology 28:573–597. https://doi.org/10.1111/j.1365-3091.1981.tb01702.x
Markello JR, Read JF (1982) Upper Cambrian intrashelf basin, Nolichucky Formation, southwest Virginia Appalachians. AAPG Bull 66:860–878
McKenzie NR, Hughes NC, Myrow PM, Choi DK, Park T-y (2011) Trilobites and zircons link north China with the eastern Himalaya during the Cambrian. Geology 39:591–594. https://doi.org/10.1130/g31838.1
Meng X, Ge M, Tucker ME (1997) Sequence stratigraphy, sea-level changes and depositional systems in the Cambro-Ordovician of the north China carbonate platform. Sediment Geol 114:189–222. https://doi.org/10.1016/s0037-0738(97)00073-0
Möller NK, Kvingan K (1988) The genesis of nodular limestones in the Ordovician and Silurian of the Oslo region (Norway). Sedimentology 35:405–420. https://doi.org/10.1111/j.1365-3091.1988.tb00994.x
Morse JW, Gledhill DK, Millero FJ (2003) $CaCO_3$ precipitation kinetics in waters from the great Bahama bank: implications for the relationship between bank hydrochemistry and whitings. Geochim Cosmochim Acta 67:2819–2826. https://doi.org/10.1016/s0016-7037(03)00103-0
Moshier SO (1986) Carbonate platform sedimentology, upper Cambrian Richland Formation, Lebanon Valley, Pennsylvania. J Sediment Petrol 56:204–216
Munnecke A, Samtleben C (1996) The formation of micritic limestones and the development of limestone-marl alternations in the Silurian of Gotland, Sweden. Facies 34:159–176. https://doi.org/10.1007/BF02546162
Myrow PM, Tice L, Archuleta B, Clark B, Taylor JF, Ripperdan RL (2004) Flat-pebble conglomerate: its multiple origins and relationship to metre-scale depositional cycles. Sedimentology 51:973–996. https://doi.org/10.1111/j.1365-3091.2004.00657.x
Myrow PM, Chen J, Snyder Z, Leslie S, Fike D, Fanning M, Yuan J, Tang P (2015) Depositional history, tectonics, and provenance of the Cambrian-Ordovician succession in the western margin of the north China Block. Geol Soc Am Bull 127:1174–1193. https://doi.org/10.1130/B31228.1
Nohl T, Munnecke A (2019) Reconstructing time and diagenesis of limestone-marl alternations from the selective compaction of colonies of the tabulate coral *Halysites*. Bull Geosci 94:279–298. https://doi.org/10.3140/bull.geosci.1752
Nohl T, Jarochowska E, Munnecke A (2019) Revealing the genesis of limestone-marl alternations: a taphonomic approach. Palaios 34:15–31. https://doi.org/10.2110/palo.2018.062
O'Brien NR (1990) Significance of lamination in Toarcian (lower Jurassic) shales from Yorkshire, Great Britain. Sediment Geol 67:25–34. https://doi.org/10.1016/0037-0738(90)90025-O
O'Brien NR (1996) Shale lamination and sedimentary processes. In: Kemp AES (ed) Paleoclimatology and paleoceanography from laminated sediments. Geological Society of London special publications, vol 116. Geological Society of London, London, pp 23–36. https://doi.org/10.1144/GSL.SP.1996.116.01.04
Park J, Lee J-H, Hong J, Choh S-J, Lee D-C, Lee D-J (2015) An upper Ordovician sponge-bearing micritic limestone and implication for early Palaeozoic carbonate successions. Sediment Geol 319:124–133. https://doi.org/10.1016/j.sedgeo.2015.02.002
Pfeil RW, Read JF (1980) Cambrian carbonate platform margin facies, Shady Dolomite, southwestern Virginia, U.S.A. J Sediment Petrol 50:91–116. https://doi.org/10.1306/212F7978-2B24-11D7-8648000102C1865D
Pohler SML, James NP (1989) Reconstruction of a lower/middle Ordovician carbonate shelfmargin: Cow Head Group, Western Newfoundland. Facies 21:189–262. https://doi.org/10.1007/BF02536836
Pratt BR, Bordonaro OL (2007) Tsunamis in a stormy sea: middle Cambrian inner-shelf limestones of western Argentina. J Sediment Res 77:256–262. https://doi.org/10.2110/jsr.2007.032
Pratt BR, James NP (1986) The St George Group (Lower Ordovician) of western Newfoundland: tidal flat island model for carbonate sedimentation in shallow epeiric seas. Sedimentology 33:313–343. https://doi.org/10.1111/j.1365-3091.1986.tb00540.x
Rankey EC, Walker KR, Srinivasan K (1994) Gradual establishment of Iapetan "passive" margin sedimentation: Stratigraphic consequences of Cambrian episodic tectonism and eustasy, southern Appalachians. J Sediment Res B64:298–310. https://doi.org/10.1306/D4267FB4-2B26-11D7-8648000102C1865D
Reid RP, Macintyre IG, James NP (1990) Internal precipitation of microcrystalline carbonate: a fundamental problem for sedimentologists. Sediment Geol 68:163–170. https://doi.org/10.1016/0037-0738(90)90109-7
Reineck HE, Singh IB (1972) Genesis of laminated sand and graded rhythmites in storm-sand layers of shelf mud. Sedimentology 18:123–128. https://doi.org/10.1111/j.1365-3091.1972.tb00007.x
Reinhardt J, Hardie LA (1976) Selected examples of carbonate sedimentation, lower Paleozoic of Maryland. Maryland geological survey guidebook, vol 5. Maryland geological survey
Reitner J (1993) Modern cryptic microbialite/metazoan facies from Lizard Island (Great Barrier Reef, Australia) formation and concepts. Facies 29:3–40. https://doi.org/10.1007/BF02536915
Sami T, Desrochers A (1992) Episodic sedimentation on an early Silurian, storm-dominated carbonate ramp, Becscie and Merrimack Formations, Anticosti Island, Canada. Sedimentology 39:355–381. https://doi.org/10.1111/j.1365-3091.1992.tb02122.x
Sawyer DE, Flemings PB, Buttles J, Mohrig D (2012) Mudflow transport behavior and deposit morphology: role of shear stress to yield strength ratio in subaqueous experiments. Mar Geol 307–310:28–39. https://doi.org/10.1016/j.margeo.2012.01.009

Schieber J, Yawar Z (2009) A new twist on mud deposition—mud ripples in experiment and rock record. Sediment Rec 7:4–8. https://doi.org/10.2110/sedred.2009.2

Sepkoski JJ Jr (1982) Flat pebble conglomerates, storm deposits, and the Cambrian bottom fauna. In: Einsele G, Seilacher A (eds) Cyclic event and stratification. Springer-Verlag, Berlin, pp 371–388

Sepkoski JJ Jr, Bambach RK, Droser ML (1991) Secular changes in Phanerozoic event bedding and the biological overprint. In: Einsele G, Richen W, Seilacher A (eds) Cycles and events in stratigraphy. Springer, Berlin, pp 298–312

Shanmugam G, Benedict GL (1978) Fine-grained carbonate debris flow, Ordovician basin margin, southern Appalachians. J Sediment Petrol 48:1233–1240. https://doi.org/10.1306/212F7644-2B24-11D7-8648000102C1865D

Shinn EA, Steinen RP, Lidz BH, Swart PK (1989) Whitings, a sedimentologic dilemma. J Sediment Petrol 59:147–161. https://doi.org/10.1306/212F8F3A-2B24-11D7-8648000102C1865D

Sohn JW, Choi DK (2005) Revision of the upper Cambrian trilobite biostratigraphy of the Sesong and Hwajeol formations, Taebaek Group, Korea. J Paleontol Soc Korea 21:195–200

Sohn JW, Choi DK (2007) Furongian trilobites from the *Asioptychaspis* and *Quadraticephalus* zones of the Hwajeol Formation, Taebaeksan Basin, Korea. Geosci J 11:297–314. https://doi.org/10.1007/BF02857047

Southard JB, Boguchwal LA (1990) Bed configurations in steady unidirectional water flows. Part 2. Synthesis of flume data. J Sediment Petrol 60:658–679. https://doi.org/10.1306/212F9241-2B24-11D7-8648000102C1865D

Srinivasan K, Walker KR (1993) Sequence stratigraphy of an intrashelf basin carbonate ramp to rimmed platform transition: Maryville Limestone (middle Cambrian), southern Appalachians. Geol Soc Am Bull 105:883–896. https://doi.org/10.1130/0016-7606(1993)105%3c0883:ssoaib%3e2.3.co;2

Trabucho-Alexandre J, Dirkx R, Veld H, Klaver G, de Boer PL (2012) Toarcian black shales in the Dutch Central Graben: record of energetic, variable depositional conditions during an oceanic anoxic event. J Sediment Res 82:104–120. https://doi.org/10.2110/jsr.2012.5

Trotter JA, Williams IS, Barnes CR, Lecuyer C, Nicoll RS (2008) Did cooling oceans trigger Ordovician biodiversification? Evidence from conodont thermometry. Science 321:550–554. https://doi.org/10.1126/science.1155814

Warnke K (1995) Calcification processes of siliceous sponges in Viséan Limestones (Counties Sligo and Leitrim, northwestern Ireland). Facies 33:215–228. https://doi.org/10.1007/BF02537453

Westphal H (2006) Limestone–marl alternations as environmental archives and the role of early diagenesis: a critical review. Int J Earth Sci 95:947–961. https://doi.org/10.1007/s00531-006-0084-8

Westphal H, Head MJ, Munnecke A (2000) Differential diagenesis of rhythmic limestone alternations supported by palynological evidence. J Sediment Res 70:715–725. https://doi.org/10.1306/2DC40932-0E47-11D7-8643000102C1865D

Westphal H, Munnecke A, Böhm F, Bornholdt S (2008) Limestone-marl alternations in epeiric sea settings—witnesses of environmental changes, or of rhythmic diagenesis? In: Holmden C, Pratt BR (eds) Dynamics of epeiric seas. Geological Association of Canada special paper, vol 48. Geological Association of Canada, pp 389–406

White WS (1943) Occurrence of manganese in eastern Aroostook County, Maine. Geological survey bulletin, vol 940-E. US Government Printing Office, Washington, D.C.

Wilson MA, Palmer TJ, Guensburg TE, Finton CD, Kaufman LE (1992) The development of an early Ordovician hardground community in response to rapid sea-floor calcite precipitation. Lethaia 25:19–34. https://doi.org/10.1111/j.1502-3931.1992.tb01789.x

Wright VP, Cherns L (2016a) How far did feedback between biodiversity and early diagenesis affect the nature of early Palaeozoic sea floors? Palaeontology 59:753–765. https://doi.org/10.1111/pala.12258

Wright VP, Cherns L (2016b) Leaving no stone unturned: the feedback between increased biotic diversity and early diagenesis during the Ordovician. J Geol Soc 173:241–244. https://doi.org/10.1144/jgs2015-043

Zhang Y, Chen D, Zhou X, Guo Z, Wei W, Mutti M (2015) Depositional facies and stratal cyclicity of dolomites in the lower Qiulitag Group (upper Cambrian) in northwestern Tarim Basin, NW China. Facies 61:417. https://doi.org/10.1007/s10347-014-0417-1

Zhou Z-C, Willems H, Li Y, Luo H (2011) A well-preserved carbonate tempestite sequence from the Cambrian Gushan Formation, eastern North China Craton. Palaeoworld 20:1–7. https://doi.org/10.1016/j.palwor.2010.12.001

Zhuravlev AY, Wood RA (2008) Eve of biomineralization: controls on skeletal mineralogy. Geology 36:923–926. https://doi.org/10.1130/g25094a.1